Journal of Alloys and Compounds 920 (2022) 165914

Contents lists available at ScienceDirect

Journal of Alloys and Compounds

journal homepage: www.elsevier.com/locate/jalcom

Research article

Evidence for cluster glass ground state in the potential giant dielectric constant material $Ba(Fe_{1/2}Sn_{1/2})O_{3-\delta}$

Arun Kumar[a,*], Girish Sahu[b], Sunil Nair[a]

[a] Department of Physics, Indian Institute of Science Education and Research, Pune 411008, India
[b] Central Instrument Facility, Indian Institute of Technology (BHU), Varanasi 221005, India

ARTICLE INFO

Article history:
Received 31 January 2022
Received in revised form 27 April 2022
Accepted 15 June 2022
Available online 18 June 2022

Keywords:
Complex perovskit
Magnetic ground state
Strongly correlated systems
Spin glass
Cluster glass

ABSTRACT

We report the magnetic ground state of the technologically important giant dielectric constant material Ba$(Fe_{1/2}Sn_{1/2})O_{3-\delta}$ (BFSO) using detailed dc and ac magnetization and specific heat measurements. Our careful x-ray diffraction analysis confirms that BFSO is single phase and crystallizes in the cubic structure with the $Pm\bar{3}m$ space group. Temperature-dependent dc susceptibility measurements reveal that magnetic irreversibility sets in below T_{irr} ~ 18 K. In addition, the zero-field cooled susceptibility exhibits a peak at the freezing temperature T_f ~ 16 K, which is also characterized by a frequency dispersion in ac susceptibility measurements. This data also confirms to the critical slowing down model with cluster-glass transition temperature T_G ~15.7 K and characteristic relaxation time τ_o ~10^{-7} s. The magnetic field dependence of the freezing temperature T_f obeys de Almeida-Thouless line in the H-T plane. The presence of aging effect and extremely slow time decay of thermoremanent magnetization is also observed below T_f. The magnetic contribution to the specific heat (C_m) exhibits a linear temperature dependence below T_f. All these observations unambiguously confirm a cluster-glass magnetic ground state in this system.

1. Introduction

The complex perovskites with general formula of the type $A(B'_xB''_{1-x})O_3$, where A is a divalent or trivalent cations and B′ and B′′ are two different cations, have attracted a lot of attention due to their interesting multi-functional properties and potential for technological applications [1–7]. Among the complex perovskites family, the Fe-containing Pb-based systems of the type $Pb(Fe_{1/2}B_{1/2})O_3$ where B = Nb, Ta and Sb, have been widely investigated due to their multiferroicity and lead iron niobate $Pb(Fe_{1/2}Nb_{1/2})O_3$ (PFNO) emerged as a model type-I multiferroic compound [8–12] in which the d^0-ness of the Nb^{5+} cation and $6s^2$ lone-pairs of the Pb^{2+} is believed to drive the ferroelectricity [8,9,13] while the d^5-ness of the Fe^{3+} ion promotes the magnetic ordering [14–16]. It exhibits a ferroelectric phase transition (T_C) ~380 K [8,9], long-range ordered (LRO) antiferromagnetic (AFM) phase transition (T_N) ~ 150 K [14–16] and a spin-glass transition (T_G) ~ 10 K [14–16]. Further, the LRO AFM phase transition is manifested by a jump in the temperature dependent dielectric constant [10] and anomalies in the unit cell lattice parameters [17] suggesting magneto-dielectric and magneto-elastic couplings. The magnetic ground state of PFNO corresponds to coexistence of LRO AFM and spin-glass phases [14,15].

On the otherhand, Pb-free complex perovskites of the type $A(Fe_{1/2}B_{1/2})O_3$ where A = Ba, Sr and Ca and B = Nb, Ta and Sb, are not multiferroic but they are known to exhibit nearly temperature stable giant dielectric constant over a broad temperature and frequency range [18–21] which is extremely attractive for miniaturization of modern electronic devices. In addition, they exhibit a dielectric relaxation step ~ 150 K where the dielectric constant drops several orders of magnitude without any structural phase transition similar to the famous quadrupole system $CaCu_3Ti_4O_{12}$ [22,23]. These complex perovskites also exhibit a strong frequency dispersion in the high-temperature region (400–650 K) [18–21]. The relaxation time (τ) corresponding to both low and high-temperature dynamics follows Arrhenius law [18–21] suggesting a non-relaxor behavior of these perovskites. Relaxors are known to follows Vogel-Fulcher law type relaxation dynamics with a critical dipolar freezing temperature (T_{VF}) at which τ diverges [24]. In contrast to Pb-based complex perovskites, the Pb-free systems do not show any LRO AFM transition [25–31]. The presence of LRO AFM transition in Pb-based system has been attributed to be due to presence of $6s^2$ lone pair orbital of Pb^{2+} which provides additional superexchange pathways Fe^{3+}-Pb^{2+}-Fe^{3+} along the < 111 > pseudocubic direction in addition to the Fe^{3+}-O^{2-}-Fe^{3+} pathways common to both the families [32]. The magnetic

* Corresponding author.
E-mail address: akm1687@gmail.com (A. Kumar).

https://doi.org/10.1016/j.jallcom.2022.165914
0925-8388/

ground state of Pb-free system corresponds to a cluster glass resulting from the freezing of the short-range ordered AFM clusters with T_G ~ 20–30 K [25–31].

In this context, barium ferrostannate $Ba(Fe_{1/2}Sn_{1/2})O_{3-\delta}$ (BFSO) is considered as a technologically important material for prospective applications. Recently, Bikyashev et al. [36] have reported a giant dielectric permittivity ($\varepsilon' \sim 10^4$) in BFSO at room temperature which makes this material attractive for applications like multifunctional devices, sensors, high density energy storage etc [33–35]. The parent $BaFeO_{3-\delta}$ is reported to exhibit series of polymorphic phases depending upon the anionic vacancy concentration (δ) [37–42] and the hexagonal phase becomes most stable at ambient condition [40–42]. Sagdeo et al. [41] first reported a colossal dielectric permittivity ($\varepsilon' \sim 10^7$) in the hexagonal phase of $BaFeO_{3-\delta}$ and its possible origin has been linked to the magnetic correlations through magneto-dielectric effect. It is noteworthy that the dielectric permittivity reported by Sagdeo et al. [41] for $BaFeO_{3-\delta}$ (with $\delta = 0.2$) at room temperature is approximately two orders of magnitude higher than the famous quadrupole $CaCu_3Ti_4O_{12}$ system [22,23]. Subsequently, Ahmed et al. [42] also investigated the isostructural $BaFeO_{3-\delta}$ (with $\delta = 0.29$) and observed a significantly lower value of dielectric permittivity $\varepsilon' \sim 10^4$ compared to that reported in $BaFeO_{2.8}$ [41]. More recently, Dang et al. [43] studied the effect of Ti-doping on $BaFeO_{3-\delta}$ and observed a very high value of dielectric permittivity (~10^4) which is comparable to other Fe-based complex perovskite systems [18–21].

Apart from the interesting dielectric behaviour, the bulk $BaFeO_{3-\delta}$ undergoes a magnetic transition from paramagnetic to AFM at T_N ~ 160 K [40]. Based on Mössbauer spectroscopy and dc magnetization studies, Iga et al. [44] proposed that the magnetic state of $BaFeO_{3-\delta}$ below T_N is not a simple long-range AFM order but a coexistence of the long-range AFM order with short-range magnetic domains. This scenario was further supported by microscopic measurement techniques like neutron scattering and muon spin relaxation [40]. Interestingly, across the long-range AFM ordering transition of $BaFeO_{3-\delta}$, several phenomena, such a sharp rise in resistivity, a huge drop in the dissipation factor (tanδ) and a peak in magneto-resistance, were observed [41]. All these observations indicate the coupling of charge and spin degrees of freedom, and lead to magneto-dielectric effect in $BaFeO_{3-\delta}$.

The present investigation was undertaken to understand the magnetic ground state of BFSO. There are two reports [45,46] on the magnetic studies of BFSO which are contradictory to each other. Roh et al. [45] did not observed any magnetic transition in BFSO except the irreversibility of the ZFC and FC M (T) curves while the second report by Bikyashev et al. [46] showed two magnetic transitions ~ 55 K and ~ 15 K, respectively. Based on the irreversibility of the ZFC and FC M (T) curves, a glass like behaviour has been tentatively proposed [45,46]. Since such irreversibility phenomena could also occur in superparamagnets [47] or even in LRO systems due to large magnetocrystalline anisotropy [48], the proposal of glassy ground state is not conclusive. It is therefore imperative to establish the existence or otherwise of the glassy ground state in BFSO using multiple criteria [49–51].

We present here comprehensive investigation of BFSO using x-ray diffraction, dielectric, dc and ac magnetizations and specific heat measurements. Our detailed analysis confirm the cluster glass ground state of BFSO.

2. Experimental details

Single phase $Ba(Fe_{1/2}Sn_{1/2})O_{3-\delta}$ (BFSO) ceramic sample was prepared by standard solid-state reaction method. Stoichiometric amount of initial ingredients $BaCO_3$, Fe_2O_3 and SnO_2 (Sigma Aldrich; ≥ 99.9%) were first thoroughly mixed using an agate mortar and pestle for 8 hrs and subsequently the mixture was calcined in an alumina crucible at 1523 K for 10 hrs. The calcined powder was grounded into fine powders and pressed into pellets of 10 mm diameter and approximately 1.0 mm thickness at a load of 90 kN. Finally, the pellets were sintered in a platinum foil at 1573 K for 3 hrs in air. The surfaces of the pellets were cleaned and crushed into fine powders and then annealed at 773 K for 12 hrs before recording the XRD patterns. The experimental density of the sintered pellets was found in the range 94–96% of the theoretical density.

The grain size distribution and chemical compositions of the BFSO were determined by scanning electron microscope (SEM) (Zeiss, model no. EVO 18) equipped with energy dispersive X-ray spectroscopy (EDS) analyzer (Oxford, model no. 51-ADD0048). The oxygen composition in the BFSO was determined by the redox iodometric titration method. X-ray diffraction (XRD) measurements were carried out using a high-resolution powder diffractometer (Bruker, model no. D8 ADVANCE). The XRD data were collected on the annealed powders in the 2θ range 20–92 degrees at a step size of 0.01 with a scan time per step of 2 s. Rietveld refinement of XRD data was carried out using FullProf package [52]. DC magnetization measurements were carried out as a function of temperature (T), and field (H) using vibrating sample magnetometer (VSM) attachment in the physical properties measurement system (PPMS, Quantum Design, USA). AC susceptibility measurements were carried out as a function of temperature at different frequencies (f) using the SQUID based magnetic properties measurement system (MPMS, Quantum Design, USA). The time (t) dependent thermoremanent magnetization (TRM) and aging measurements were also performed using the same instrument. The temperature dependent specific heat measurements were performed on a PPMS set-up with HC module. For this, we first performed the addenda (platform + apiezone N-grease) measurement and then specific heat measurement of sample (i.e., sample + platform + apiezone N-grease) using a small piece of the sintered pellet. The absolute value of the specific heat of the sample was obtained by subtracting the value of specific heat of addenda from the total measured specific heat. The temperature dependent dielectric measurements of BFSO were carried out using Novocontrol high-performance frequency analyzer and a close cycle refrigerator (CCR) based system. For the dielectric measurements, the top and bottom surfaces of the pellet were painted with silver paste. The dielectric data were collected at a heating rate of 0.5 K/minute with a step size of 2 K.

3. Results and discussion

3.1. Microstructure, chemical homogeneity and room temperature crystal structure

The scanning electron micrograph image of BFSO shown in Fig. 1(a) reveals highly dense microstructure free from pores. Well-defined grains separated by grain boundaries are clearly seen in the microstructure. We determine the grain size distribution by considering large number of grains in the microstructure. A histogram showing the grain size distribution is depicted in the inset of Fig. 1(a). It is evident that the average grain size of BFSO is ~ (0.91 ± 0.33) μm. We have also performed microstructural analysis using Williamson-Hall (W-H) plot method to estimate the average crystallite size and lattice strain of the BFSO. The Williamson-Hall relation can be expressed as [53]:

$$\beta \cos\theta = k\,\lambda / d + 4\,\alpha \sin\theta \quad (1)$$

where β is the full width at half maxima (FWHM), θ the Bragg's angle, k is a Scherrer constant and is in general equal to 0.90 for powders, d is average value of crystallite size, λ is wavelength of radiation (For CuK_α, $\lambda = 1.5406$ Å) and α is average value of lattice strain. To determine the intrinsic FWHM of the sample, we have

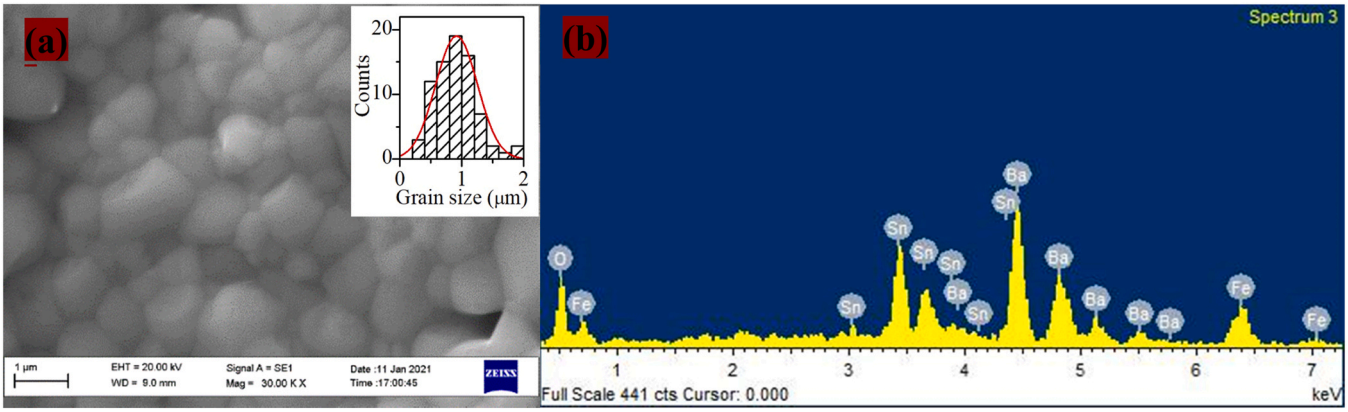

Fig. 1. (a) Scanning electron micrograph showing the microstructure of $Ba(Fe_{1/2}Sn_{1/2})O_{3-\delta}$. Inset depicts the histogram of grain size distribution with the Gaussian fitting (red curve). (b) The representative energy dispersive x-ray spectrum showing the presence of Ba, Fe, Sn and O elements in the $Ba(Fe_{1/2}Sn_{1/2})O_{3-\delta}$ sample.

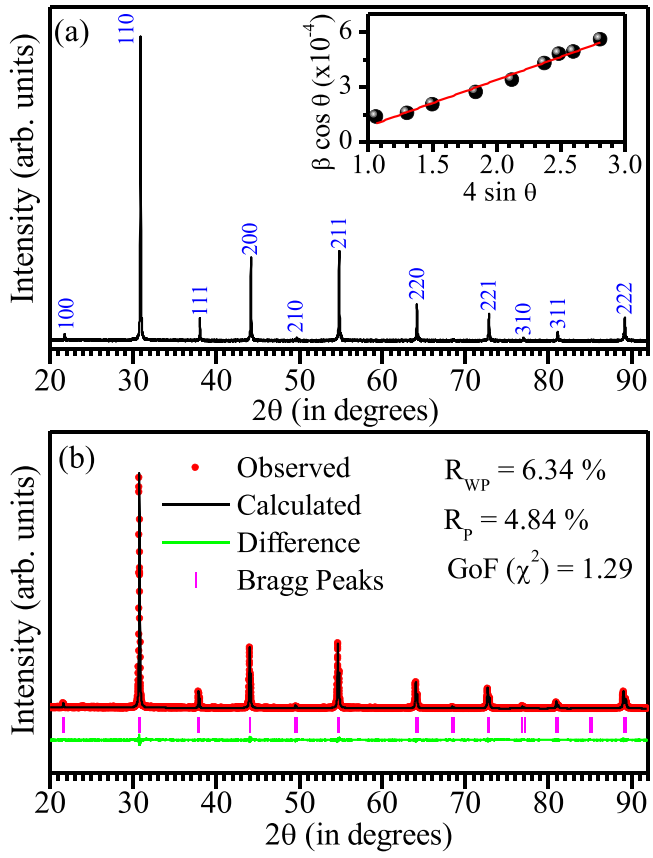

Fig. 2. (a) X-ray powder diffraction pattern of $Ba(Fe_{1/2}Sn_{1/2})O_{3-\delta}$ at room temperature with CuKα radiation (λ = 1.5406 Å). All the indices are written with respect to the cubic perovskite cell. Inset shows the Williamson-Hall plot for $Ba(Fe_{1/2}Sn_{1/2})O_{3-\delta}$. (b) Fitting of the observed (red dots) and calculated (black continuous line) patterns using cubic $Pm\bar{3}m$ space group. The green continuous line represents the difference between the observed and calculated profiles. The vertical bars above the difference line indicate the allowed position of Bragg peaks.

subtracted the instrumental broadening effect using a standard LaB_6 sample. The W-H plot (β cosθ versus 4 sinθ) obtained from the XRD pattern of BFSO after removing the $K\alpha_2$ contribution is shown in the inset of Fig. 2(a). The average crystallite size and lattice strain obtained from the straight-line fit are ~ (0.83 ± 0.11) μm and (2.5 ± 0.1) × 10^{-4}, respectively. The average grain size obtained from the SEM micrograph is in close agreement with the crystallite size determined from the W-H plot.

To check the chemical composition, EDS spectra of BFSO were recorded at randomly selected regions in the microstructure and a representative spectrum is shown in Fig. 1(b), which reveal peaks corresponding to Ba, Fe, Sn and O. Here, we have excluded the oxygen composition in EDS analysis as this technique is less sensitive to low atomic number (Z) element like O. The results of EDS analysis after averaging over 18 different regions are given in Table 1. It can be seen from this table that the observed chemical composition of Ba, Fe, and Sn are in excellent agreement with the nominal composition within the standard deviation. The oxygen content in the BFSO estimated from the redox iodometric titration method is deduced to be (2.76 ± 0.01) with δ = (0.24 ± 0.01) which is in perfect agreement with the previous report [45]. Keeping charge neutrality and oxygen stoichiometry into consideration, the full electronic composition formula for BFSO sample is $Ba^{2+}(Fe^{3+}_{0.48}Fe^{4+}_{0.02}\ Sn^{4+}_{0.50})O^{2-}_{2.76}$. We will discuss the impact of oxygen deficiency in the physical and magnetic properties of BFSO in the later sections.

Fig. 2(a) shows the high-resolution XRD pattern of BFSO after stripping of the $K\alpha_2$ contribution. In conformity with the previous report [36], the XRD pattern of BFSO reveals the formation of a single-phase perovskite with no traces of any impurity phase. All the peaks in the diffraction pattern of BFSO could be indexed with a cubic perovskite cell. This was further confirmed by the Rietveld refinement technique using XRD data shown in Fig. 2(b). The observed and calculated profiles show excellent fit for the cubic $Pm\bar{3}m$ space group, as can be seen from the nearly flat difference profile. The so-obtained lattice parameters and unit cell volume a = b = c = 4.1106 (3) Å and V = 69.456 (1) $Å^3$, respectively, are consistent with an earlier report [36].

3.2. Dielectric behaviour

Fig. 3(a) and 3(b) depict the variation of real part of dielectric permittivity (ε′) and loss tangent (tanδ) for BFSO as a function of frequency at room temperature. It can be seen that the dielectric permittivity decreases continuously with increasing frequency while the tanδ first decreases up to 100 Hz frequency and then increases slightly (~3000 Hz) followed by gradual decrease with increasing

Table 1
Quantification of $Ba(Fe_{1/2}Sn_{1/2})O_{3-\delta}$ by EDS analysis performed at 18 randomly selected regions in the microstructure.

Element	Average chemical composition in Atomic %	
	Expected	Observed
Ba	50	50.4 ± 1.7
Fe	25	24.5 ± 2.2
Sn	25	25.1 ± 1.4

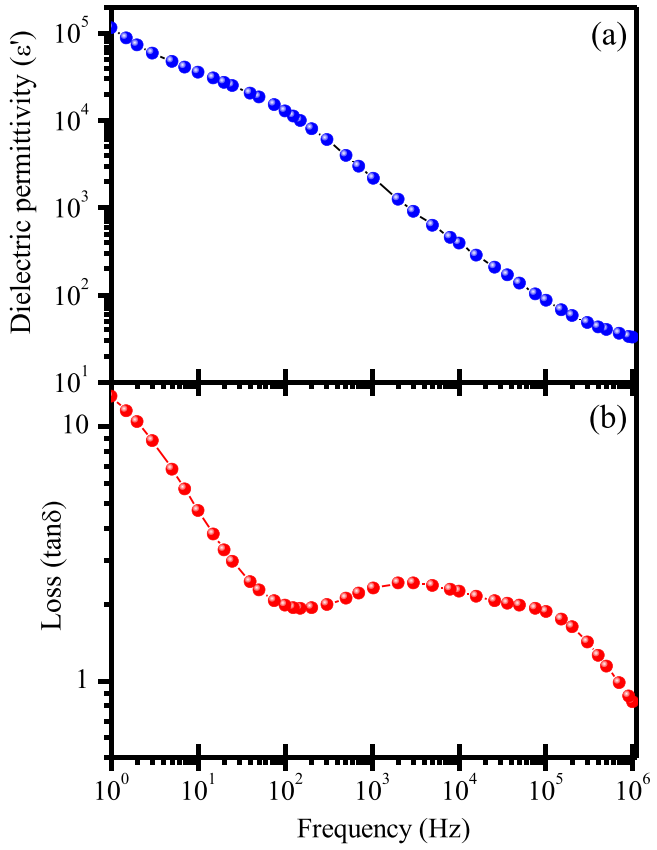

Fig. 3. Variation of (a) dielectric permittivity (ε') and (b) loss tangent (tan δ) as a function of frequency at room temperature for $Ba(Fe_{1/2}Sn_{1/2})O_{3-\delta}$.

frequency. A similar behaviour of dielectric permittivity and tanδ were also reported in Fe-containing B-site disordered perovskites $A(Fe_{1/2}B_{1/2})O_3$ where A = Ba, Sr, Ca and B = Nb, Ta, Sb [18]. Our room temperature values of ε′ ~1.2×10^4 and tanδ ~1.9 at 100 Hz for BFSO are comparable to that reported recently by Bikyashev et al. [36]. These values agree well with the parent compound $BaFeO_{3-\delta}$ (ε′ ~10^4) [42], Ti-doped $BaFeO_{3-\delta}$ (ε′ ~10^4) [43] and CCTO (ε′ ~10^4 –10^5) [22,23]. It is noteworthy that, Sagdeo et al. [41] reported orders of magnitude larger value of ε′ ~ 10^7 and very large tanδ ~ 20 at 10 kHz for $BaFeO_{3-\delta}$.

To further explore the relaxation mechanism involved in BFSO, we performed temperature dependent dielectric measurements. Fig. 4(a) and 4(b) show the temperature dependence of the real part of dielectric permittivity (ε' (T)) and loss tangent (tanδ (T)) of BFSO at different measuring frequencies. It can be seen that the ε'(T) shows nearly temperature and frequency independence behaviour upto a certain temperature (for example ~175 K at 101 Hz), and then it starts increasing gradually (upto ~240 K for 101 Hz) followed by a sharp increase in ε'(T). On the otherhand, tanδ (T) exhibit two peaks in this temperature range suggesting the presence of two dielectric relaxations (hereafter labelled as the LT_1 and LT_2). Similar two relaxation processes were also observed in $BaFeO_{3-\delta}$ [41] and Ti-doped $BaFeO_{3-\delta}$ [43] below room temperature. It is interesting to note that both peaks in tanδ show frequency dispersion. To analyze the temperature dependence of two dielectric relaxations of BFSO, we used first derivative plots of tanδ which exhibit two peaks T_1 and T_2 (see Fig. S1 of the supplemental information for more details). Interestingly, the peak temperatures T_1 and T_2 corresponding to two relaxations shift to higher temperature with increasing frequency. The frequency dependent dielectric relaxations may arise due to relaxor ferroelectric transition or Maxwell-Wagner type relaxations at the grain boundaries and internal imperfections [3,24]. The frequency dependent shift ΔT is rather huge in both dielectric relaxations and we proceed to analyze the origin. The Maxwell-Wagner type relaxation usually follows Arrhenius law [18],

$$\tau = \tau_0 \exp[E_a/k_BT] \quad (2)$$

where E_a is the thermal activation energy, τ_0 is the characteristic relaxation time, k_B is the Boltzmann's constant. On the otherhand, the relaxation time (τ) in relaxor ferroelectrics follows the empirical Vogel-Fulcher law [3,24],

$$\tau = \tau_0 \exp[E_a/k_B(T-T_{VF})] \quad (3)$$

where T_{VF} is the Vogel-Fulcher freezing temperature. The temperature dependence of both the dielectric relaxations of BFSO follows the Arrhenius law. This is confirmed by the ln (τ) versus 1/T plots shown in Fig. 4(c) and 4(d). The straight-line nature of the plot suggests Arrhenius behaviour and non-relaxor ferroelectric nature of BFSO with activation energies E_{a1} =(0.28 ± 0.01) eV, E_{a2} =(0.44 ± 0.01) eV and relaxation time τ_{01} =(1.1 ± 0.2) $x10^{-11}$ s, τ_{02} =(4.4 ± 1.2)$x10^{-13}$ s, respectively, for the two relaxations. The estimated value of E_{a1} corresponding to LT_1 relaxation of BFSO is close to the activation energy of polaronic relaxation (E_a ~ 0.14 –0.28 eV) caused by the localized charge carrier hopping between Fe^{4+} and Fe^{3+} ions [41,42]. It is well-known that the physical properties are strongly influenced by the oxygen vacancies which are created during sintering process at high-temperatures. As per the Kröger-Vink notation, each oxygen vacancy leaves behind two electrons [54]: $O_0 \Leftrightarrow 1/2O_2 + V_{\ddot{O}} + 2e'$ where O_0, $V_{\ddot{O}}$ and e′ represent the oxygen atom, oxygen vacancies with two net positive charges and electron with negative charge, respectively. The released electron from the oxygen vacancy may be captured by Fe^{4+} of BFSO and leading to its reduction to Fe^{3+} ($Fe^{4+} + e' \Leftrightarrow Fe^{3+}$). The presence of Fe^{4+} and Fe^{3+} ions leads to hopping phenomena in the BFSO. Furthermore, the presence of a pair of Fe^{3+}-Fe^{4+} ions may also act as defect dipoles with finite local polarization. In the presence of electric field, the polaron hopping is identical to the flipping of the dipole and hence strongly affects the dielectric behaviour. On the otherhand, the calculated activation energy E_{a2} of LT_2 relaxation of BFSO is close to the activation energy reported for $Ba(Fe_{1/2}Nb_{1/2})O_3$ (~0.35 eV) [18], $Ca(Fe_{1/2}Sb_{1/2})O_3$ (~0.40 eV) [18] and $Ba(Fe_{0.8}Ti_{0.2})O_{3-\delta}$ (~0.49 eV) [43], where the dielectric relaxation behavior has been attributed to the Maxwell-Wagner effect. Thus, we conclude that the two dielectric relaxations in BFSO originates from the polaron hopping and Maxwell-Wagner effect, respectively.

3.3. DC susceptibility

The temperature dependence of zero-field cooled (ZFC) dc magnetic susceptibility χ (T) (= M/H, where M is the magnetization and H is the applied field) of BFSO measured at 100 Oe field is shown in Fig. 5(a). Evidently, χ (T) increases gradually with decreasing temperature and shows a peak at T_f ~ 16 K which is possibly due to spin/cluster-glass freezing. On further cooling, χ (T) exhibits a shoulder around 9 K at lower field and disappear at higher field (H ≥ 1000 Oe). Such a shoulder has also been observed in the other Fe-containing complex perovskites $A(Fe_{1/2}M_{1/2})O_3$ (where A = Ba, Sr, Ca, M = Nb, Ta) [25,27,29,30]. The origin of this shoulder is unknown to us. To understand the nature of magnetic interactions in BFSO, we plot temperature dependence of inverse of ZFC susceptibility (1/χ) at 100 Oe field in Fig. 5(b). It is evident from the figure that above 200 K, χ^{-1}(T) increases linearly with temperature and follows Curie-Weiss (C-W) law [55]:

$$\chi(T) = \left(\frac{C}{T - \theta_{CW}}\right) \quad (4)$$

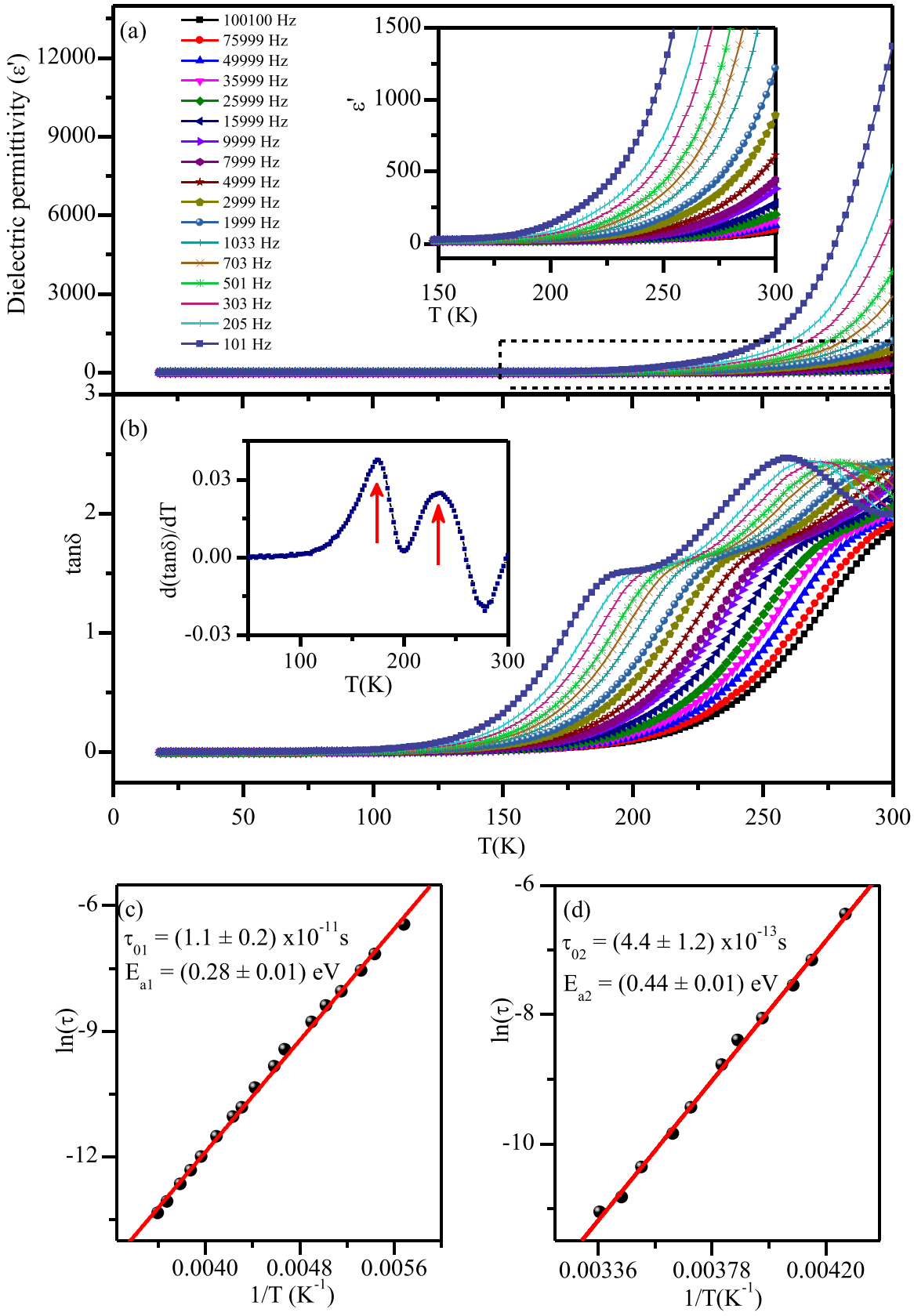

Fig. 4. Temperature dependence of (a) real part of dielectric permittivity (ε') and (b) dielectric loss (tanδ) for $Ba(Fe_{1/2}Sn_{1/2})O_{3-\delta}$ at various frequencies ranging from 0.1 kHz to 100 kHz. The inset of (a) and (b) show the magnified portion of the real part of dielectric permittivity and first derivative of loss tangent (d(tanδ)/dT) with respect to temperature at 101 Hz frequency, respectively. Panels (c) and (d) show the Arrhenius plots (ln (τ) versus 1/T) for the two dielectric relaxations.

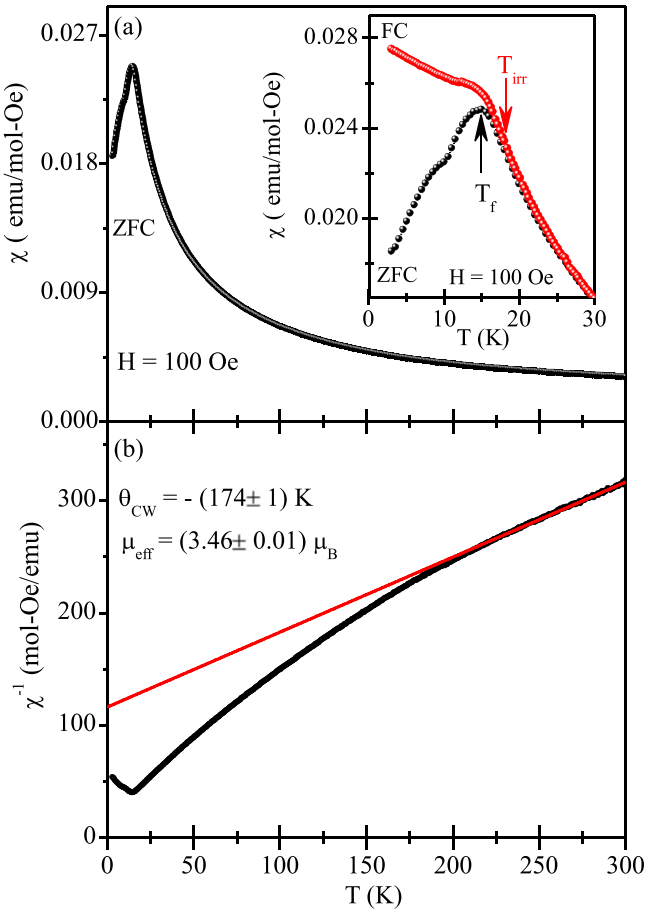

Fig. 5. Upper panel (a) Temperature dependence of zero-field cooled (ZFC) dc susceptibility χ (T) of $Ba(Fe_{1/2}Sn_{1/2})O_{3-\delta}$ measured at H= 100 Oe. Inset of panel (a) shows the temperature dependence of ZFC and FC dc susceptibility curves on a magnified scale to reveal history dependent bifurcation and a flatness/plateau in the FC χ (T) curve below T_f. Lower panel (b) depicts the inverse of ZFC dc susceptibility (χ^{-1}) versus temperature plot. The continuous line through data points represent the Curie-Weiss fit using Eq. (4) in the range 225–300 K.

where C is Curie constant and θ_{CW} is Curie-Weiss temperature. The fitting parameters obtained after the least-squares fit in the range 225–300 K are: C = (1.498 ± 0.006) emu K mol^{-1} Oe^{-1} and θ_{CW} = - (174 ± 1) K. Physically, θ_{CW} represents the sum of all exchange interactions present in the system. The negative value of θ_{CW} suggests dominant antiferromagnetic type magnetic correlations in this system. However, the departure from Curie-Weiss behaviour is notable below 175 K and points towards the possible role of short-range correlations in BFSO.

The calculated effective moment (μ_{eff}) from the Curie constant using relation $\mu_{eff} = \sqrt{\frac{3Ck_B}{N_A}}\mu_B$ comes out to be ≈ (3.46 ± 0.01) μ_B which is approximately half of the expected moment (5.916 μ_B) for the high spin Fe^{3+} (S = 5/2) state. The low value of μ_{eff} was reported in the Fe-containing niobates and tantalates compounds also [25,27,29,30] and has been attributed to be due to the presence of nanometer-size AFM clusters [29]. Higher temperature χ (T) data may provide higher μ_{eff} value close to the theoretical value after breaking the AFM correlated clusters [16].

The temperature dependence of ZFC and FC χ (T) plots of BFSO measured at 100 Oe field are shown in Fig. 5(b). Evidently, the two curves bifurcate at a characteristic temperature T_{irr} ~ 18 K with a peak in the ZFC χ (T) curve at T_f ~ 15 K. In canonical spin glasses (dilute magnetic alloys like CuMn), T_{irr} nearly coincides with the T_f while in concentrated systems (leading to cluster glasses) $T_{irr} > T_f$ [50]. The bifurcation of ZFC and FC χ (T) curves is a characteristic features of spin/cluster glasses and superparamagnetic blocking [49–51]. A notably different behaviour of FC χ (T) is expected for cluster glasses and superparamagnetic blocking [47]. The FC χ (T) of cluster glasses show a plateau below T_f and then start increasing with decreasing temperature [29,47,56] while in superparamagnetic blocking FC χ (T) increases monotonically with decreasing temperature [47]. As can be seen from the inset of Fig. 5(a), the FC χ (T) curve of BFSO shows a plateau over a small temperature range and then starts increasing with decreasing temperature suggesting the cluster-glass freezing.

3.4. AC susceptibility

To distinguish the spin/cluster glass freezing and superparamagnetic blocking, we carried out ac susceptibility measurements at different frequencies in the vicinity of freezing temperature T_f. The amplitude of ac field was fixed at 5 Oe for all measurements. Results of the real part of ac susceptibility χ'(ω, T) as a function of temperature is depicted in Fig. 6. Evidently, χ' (T) exhibits a peak across the freezing temperature $T_f(\omega)$, similar to observed in dc χ (T) (shown in panel (a) of Fig. 5). The position of the peak $T_f(\omega)$ shifts to higher temperature and the magnitude of χ' (T) decreases with increasing frequency (f). Such a frequency dependent shift of $T_f(\omega)$ has been observed in both spin/cluster glass and superparamagnets [49–51]. The two phenomena can be distinguished by analyzing the empirical Mydosh parameter defined by [50]: $\Phi = \Delta T_f / (T_f \Delta \ln(\omega))$, where ΔT_f is shift in the peak temperatures corresponding to lowest and highest frequencies. The accurate peak position was determined from the seventh order polynomial fits to the observed data shown in the Fig. 6(a). The value of Φ for BFSO comes out to be ~0.013 which is much lower than that reported for non-interacting superparamagnetic systems (0.1–0.3) and lies in the expected range of spin-glasses (0.005–0.09) [50]. Indeed, the value of Φ for BFSO is comparable to the cluster glass systems like $Cr_{0.5}Fe_{0.5}Ga$ (~ 0.017) [57], $Zn_3V_3O_8$ (~ 0.028) [58], $Ca_3Mn_3(O_2BO_3)_2$ (~ 0.02) [59], $Sr(Fe_{1/2}Nb_{1/2})O_3$ (~ 0.023) [30], $CoGa_2O_4$ (~ 0.028) [60] and $Ca(Fe_{1/2}Nb_{1/2})O_3$ (~ 0.045) [29]. Thus our Mydosh parameter analysis suggests the cluster glass freezing rather than the superparamagnetic blocking is responsible for the peak in ZFC χ (T) of BFSO.

In order to further explore the spin/cluster dynamics, we analyzed the frequency dependence of $T_f(\omega)$ using conventional "critical slowing down" model given by power law expression [49]:

$$\frac{\tau}{\tau_0} \propto \left(\frac{T_f(\omega) - T_G}{T_G}\right)^{-z\nu}, \quad (5)$$

where τ (= 1/2πf) is the relaxation time corresponding to the measurement frequency (f), τ_0 signifies the characteristic relaxation time of individual spin or cluster of spins, T_G is the critical glass transition temperature at which the ergodicity breaking occurs and the longest relaxation time τ diverges, ν is characteristic exponent of spin-spin correlation length $\xi \propto (T_f/T_G\text{-}1)^{-\nu}$ and z denotes dynamic critical exponent relating the relaxation time τ to correlation length ξ as $\tau \propto \xi^z$ [49]. In Fig. 6(b), ln (τ) versus $\ln(T_f(\omega)/T_G - 1)$ is plotted which gives very good fit for the critical slowing down model Eq. (5) with fitting parameters: T_G = (15.7 ± 0.1) K, zν = (2.4 ± 0.1) and τ_0 = (3.2 ± 0.9) x10^{-7} s, respectively. The observed value of zν for BFSO is somewhat lower than the canonical spin-glasses (4–10) [49,50] but in good agreement with the values reported for cluster glass systems like $Cu_2Mn_{0.5}Fe_{0.5}Al$ (~2.2) [61], $LuFe_2O_4$ (~2.85) [62], $Zn_3V_3O_8$ (~ 2.98) [60], $LiZn_2V_3O_8$ (~ 2.65) [63], $SmFeO_3$(~2.85) [64]. The value of τ_0 for BFSO is orders of magnitude larger than that observed in typical canonical spin glasses which usually lies in the range of 10^{-11} - 10^{-13} s [49,50]. In fact, τ_0 for BFSO is consistent with those reported in cluster glass systems in the range 10^{-6} – 10^{-10} s [29,56,62–65]. The large value of τ_0 strongly suggests presence of

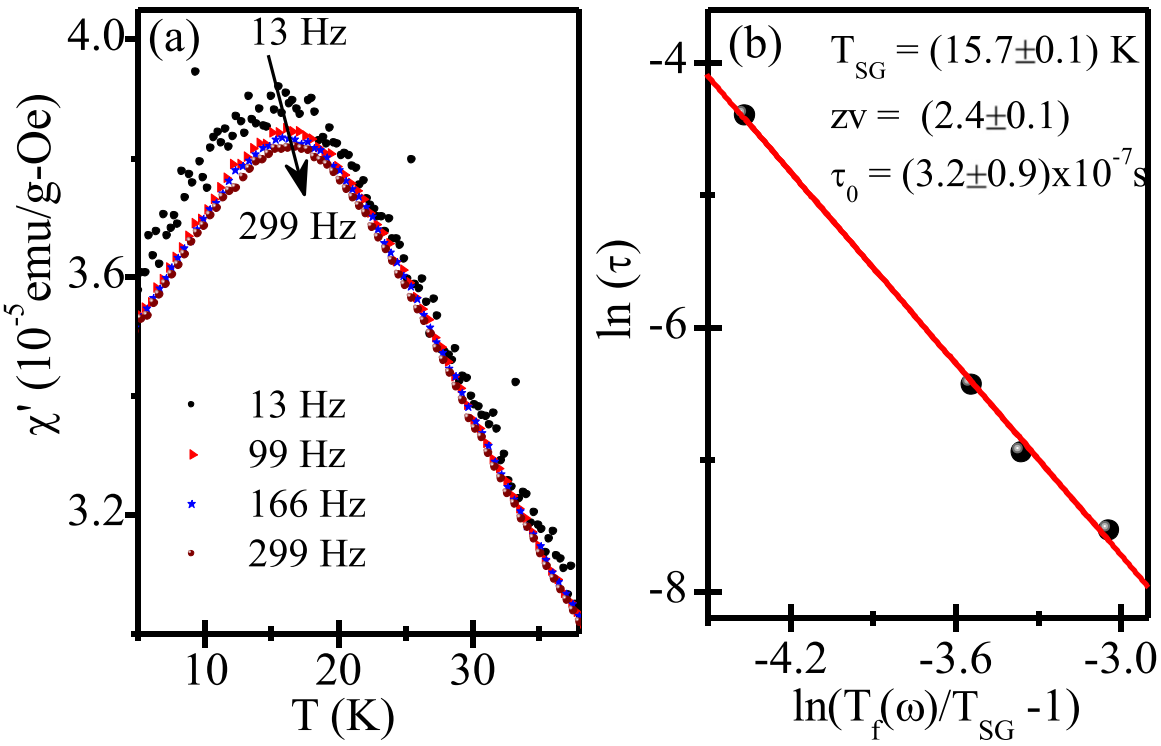

Fig. 6. Left panel (a) Temperature dependence of real part of ac susceptibility of $Ba(Fe_{1/2}Sn_{1/2})O_{3-\delta}$ at various frequencies (13 Hz, 99 Hz, 166 Hz and 299 Hz) with a fixed ac drive field of 5 Oe. Right panel (b) shows ln (τ) versus ln ($T_f(\omega)/T_{SG}$-1) plot and solid line is the fit to the critical slowing down model given by power law Eq. (5).

clusters in the BFSO system and these interacting clusters leads to glassy freezing due to frustrated nature of the exchange interactions. Thus our critical slowing down analysis of the ac susceptibility χ' (T) data confirms the cluster glass phase in BFSO with T_G ~ 15.7 K.

3.5. Isothermal magnetization

To further understand the nature of the magnetic state in BFSO, the field dependent magnetization (M versus H) curves were recorded at selected temperatures shown in Fig. 7. It is evident that the

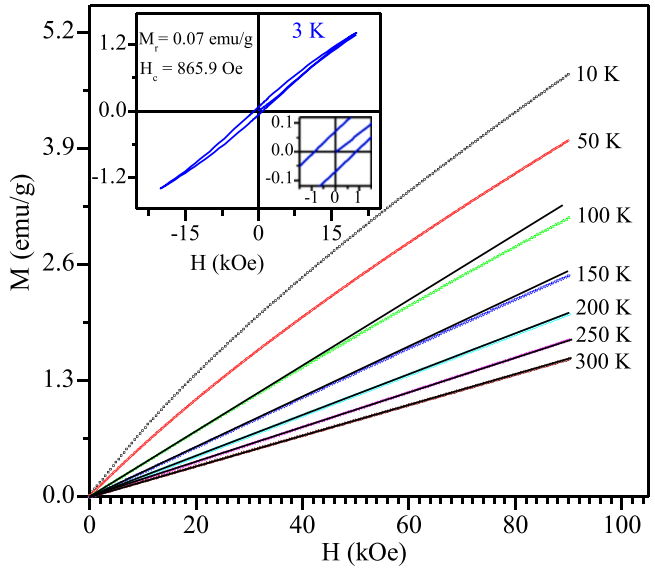

Fig. 7. The magnetization versus field curves of $Ba(Fe_{1/2}Sn_{1/2})O_{3-\delta}$ at selected temperatures 10, 50, 100, 150, 200, 250 and 300 K. The solid lines in the plot shows the deviation from the linear behavior. Inset: M versus H plot at 3 K along with magnified view in the low field region.

M-H curves exhibit linear characteristic in the temperature range 200–300 K. This clearly demonstrate the paramagnetic nature of BFSO above 200 K. A considerable non-linearity in M-H curves were observed below 200 K (see derivative plots shown in Fig. S2 of the supplemental information for more details) which suggest that some short-range order start appearing gradually with decreasing temperature. This is consistent with the Curie-Weiss behavior observed in BFSO which also shows deviation from the linearity below 200 K. Notably, the M-H curve does not show any saturation even at very high magnetic fields of 90 kOe, indicating the presence of dominant AFM interactions in the system. Interestingly, we observed a small opening of the M-H hysteresis loop with considerable remanent magnetization (M_r ~ 0.07 emu/g) and coercive field (H_c ~ 966 Oe) at 3 K (see inset of Fig. 7). Such small opening of the M-H loop has been commonly observed in spin glasses/cluster glasses below T_f [47,49–51,66] and attributed to the presence of short-range ordered FM/AFM clusters.

3.6. H-T phase diagram

To get more insight into the nature of the glassy state, we analyzed the field dependence of the freezing temperature (T_f). Despite extensive study on the spin-glass transition, a consensus about the stability of the spin-glass state in presence of magnetic field is still lacking [67] and continues to be debated as two entirely different scenarios have been proposed in the literature [68,69]. The first scenario [68] due to de Almeida-Thouless (A-T), using Sherrington-Kirkpatrick (S-K) model of infinite range interaction within the mean field approximations, predicts that the replica symmetry breaking (RSB) occurs even in the presence of low fields which shows that the spin-glass state is stable under finite magnetic field also. The second scenario of spin-glass was speculated on the basis of the phenomenological droplet model [69] in which the replica symmetry is retained and the spin-glass state is unstable in the presence of even an infinitely small magnetic field. Another independent theoretical

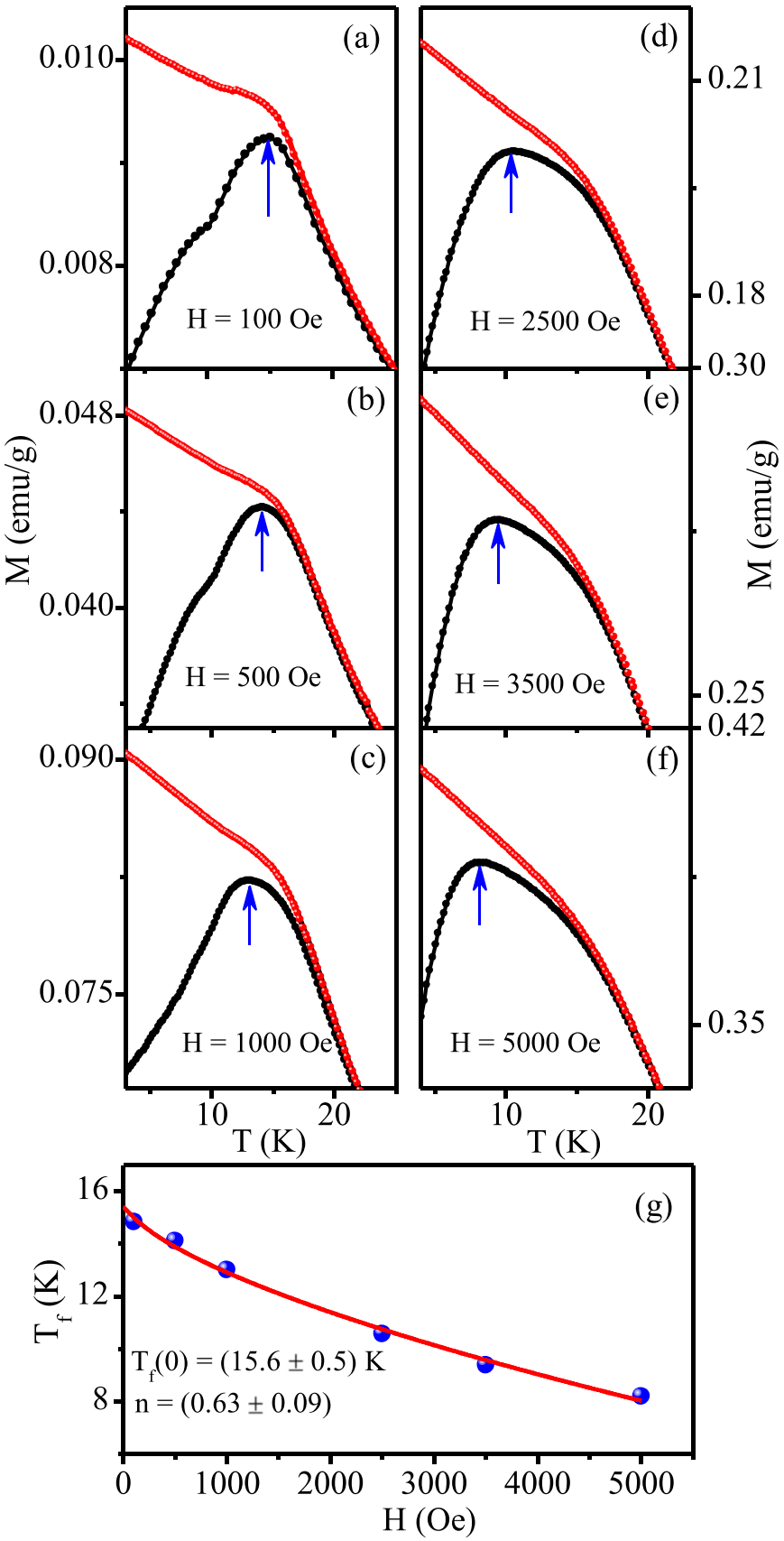

Fig. 8. Temperature dependence of the zero-field cooled (ZFC) and field-cooled (FC) dc magnetization curves for $Ba(Fe_{1/2}Sn_{1/2})O_{3-\delta}$ measured at (a) 100 Oe, (b) 500 Oe, (c) 1000 Oe, (d) 2500 Oe, (e) 3500 Oe, and (f) 5000 Oe. The arrow pointing the upwards correspond to the freezing temperature (T_f). Panel (g) Variation of T_f as a function of H. The solid line through data points is the least square fit to the theoretical predicted de Almeida-Thouless Eq. (6) with critical exponent m ~ 0.63.

study of vector spin glasses by Gabay and Toulouse and Sherrington [70,71] shows that the spin-glass phase persists in the presence of magnetic field for both Ising and Heisenberg systems. In the T-H phase diagram for the spin glass systems, de Almeida Thouless (A-T) and Gabay-Toulouse (G-T) lines have been theoretically predicted [68,70,71] with different field exponents. The field dependence of two critical lines in the T-H plane can be expressed as [68,70,71],

$$T_f(H) = T_f(0)[1 - AH^m] \quad (6)$$

where $T_f(0)$ is the freezing temperature in the limit of $H \rightarrow 0$, A is a constant and m is the critical exponent which corresponds to m = 2/3 for the A-T and m = 2 for the G-T line. Experimentally, A-T and G-T lines in the T-H plane have been constructed using field dependence of either the peak temperature (T_f) [14,29,56,72] in the ZFC M (T) plot or irreversibility temperature (T_{irr}) [29,57] where ZFC and FC M (T) curve bifurcates.

To construct T-H phase diagram of BFSO, we measured temperature dependence of ZFC and FC M (T) at different fields in the range 100–5000 Oe, as shown in Fig. 8(a-f). It is evident that the peak temperature T_f (H) corresponding to cluster glass freezing marked with arrows shifts to low temperature side with increasing magnetic field, consistent with the theoretical predictions [68] for the spin glasses as per the first scenario discussed earlier. To determine T_f more accurately, we fitted the ZFC M (T) data with 7th order polynomial function in a region close to the observed peak. The variation of T_f with magnetic field is depicted in Fig. 8(g). A least-squares fit to Eq. (6) gave the characteristic exponent m = (0.63 ± 0.09) which is in perfect agreement with the theoretically predicted value (m ~ 2/3) for A-T line within the mean field approximation [68]. The A-T type critical line represents a phase boundary between the ergodic (paramagnetic) and non-ergodic (spin-glass) phases in the T-H phase diagram. Such A-T line has been reported in well-known canonical spin-glass as well as cluster glass systems [14,29,73,74]. The extrapolation of the A-T line to H = 0 gives the T_f (H = 0) = (15.6 ± 0.5) K which is in agreement with the T_G ~ (15.7 ± 0.1) K determined from the ac susceptibility measurements. Thus the presence of A-T type critical line in the T-H plane further supports the existence of glassy phase in BFSO.

3.7. Magnetic relaxation and aging effects

It is well established that aging effects and long-time relaxation phenomena are typical characteristics of the spin/cluster glass state [49–51]. To understand these phenomena in BFSO, we performed time dependent thermoremanent magnetization (TRM) at different waiting times (t_w) below T_f. For this, we followed standard FC protocol in which the sample is cooled in presence of 100 Oe field from 300 K ($T > T_f$) to a desired wait temperature T_w ($< T_f$) = 10 K at the rate of 2 K/min. After the reaching at 10 K, the sample was allowed to age for wait time of t_w = 100 s. After the elapse of wait time t_w at 10 K, field was switched off to zero and relaxation of magnetization was recorded as a function of time. We followed the above procedure for waiting times t_w = 1000 s and 2000 s. The results of the decay of magnetization M (t) with time at different waiting times are depicted in Fig. 9. It is evident that the M (t) curve continues to decay with time and do not show saturation even after the measurement of 6500 s. The maximum decay of M (t) curve is found to be ~23% corresponding to wait time of 100 s. Such a very slow decay has been speculated to arise due to the presence of hierarchical arrangements of the metastable states separated by different energy barriers which respond to the different relaxation times after the release of magnetic field. Evidently, the decay of M (t) curve is found to be sensitive to the waiting time t_w. The longer waiting time relaxes more slowly which clearly demonstrate the aging effects in BFSO.

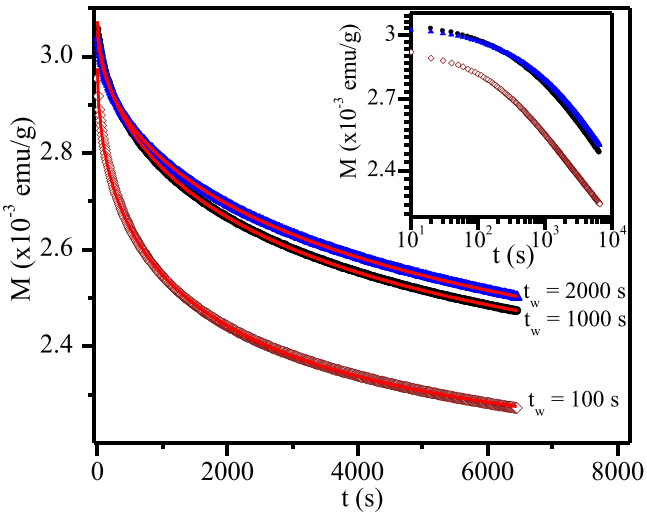

Fig. 9. Thermoremanent magnetization M (t) of $Ba(Fe_{1/2}Sn_{1/2})O_{3-\delta}$ as a function of time at 10 K for 100 Oe cooling field with different wait times (t_w = 100 s, 1000 s and 2000 s). The solid line in the plots are best fit for the stretched exponential function to the data. Inset shows the log-log plot of M (t) data with time. The non-linear nature of these plots clearly rules out the logarithmic dependence of M (t).

Theoretically, for spin/cluster glasses, Palmer et al. [75] established a stretched exponential type functional dependence of M (t) with time, based on the hierarchically constrained dynamics, which is expressed as:

$$M(t) = M_0 + M_g \exp[-(t/\tau)^{\beta}] \quad (7)$$

where M_0 is the magnetization corresponding to LRO component, M_g is the magnetization related to glassy component which contributes to the observed relaxation effects, τ is the characteristic relaxation time and β is the stretched exponent. Both τ and M_g depends on temperature as well as the waiting time t_w while the value of β is only dependent on temperature. The $\beta = 1$ corresponds to simple Debye like relaxation with a single relaxation time τ while $\beta = 0$ indicate the absence of relaxation. In the glass state, the energy landscape is multivalleyed with different potential energy barriers, the relaxation time (τ) has a distribution and value of β lies in the range $0 < \beta < 1$ [75]. We have fitted the observed M (t) versus time plots using the stretched exponential Eq. (7). This is shown by continuous solid line through data points in Fig. 9. The parameters M_0, M_g, τ and β extracted from the fit ranges from (2.15–2.25) x10^{-3} emu/g, (0.822–0.840) x10^{-3} emu/g, (1825–5821) s and 0.51–0.55, respectively, for different waiting times. The small value of M_0 reveals that the long-range ordered component in BFSO case is antiferromagnetic. Interestingly, the value of β for BFSO falls within the range of spin/cluster glasses [54,57,76]. Alternatively, a logarithmic time dependence of M (t) have been reported in some systems which is expressed as [77,78]:

$$M(t) = M_0 - C \log(t) \quad (8)$$

where M_0 is the initial remanent magnetization and C is a constant which depends on the material, temperature and field. As per Eq. (8), the log-log plots of M (t) versus time should be linear. However, the non-linear nature of the plots shown in the inset of Fig. 9 clearly rules out the applicability of the logarithmic type functional dependence in BFSO. It is interesting to note that the different linear regions are observed in the plots (see inset of Fig. 9) which point towards the existence of different relaxation times. A comparison of the M (t) versus time curves also suggests that the logarithmic type functional decay is valid only for a few decades time scales whereas the stretched exponential type decay describes

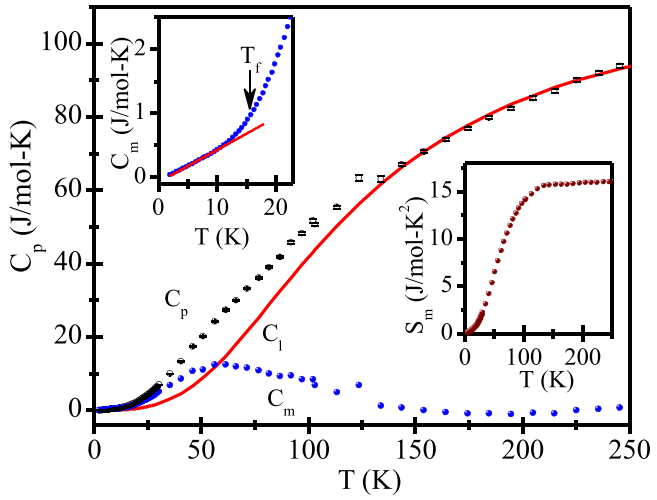

Fig. 10. The main panel depicts the temperature dependence of total specific heat (C_p: open circle) of $Ba(Fe_{1/2}Sn_{1/2})O_{3-\delta}$ at zero magnetic field along with lattice specific heat (C_l: continuous line) obtained from fitting with the Debye model (see Eq. (9)) and magnetic specific heat (C_m: filled circle) obtained by subtracting the lattice contribution from the total specific heat. The top inset shows the temperature variation of C_m in the range 2–25 K and solid line is the fit using $C_m = AT$-type dependence. Bottom inset depicts the variation of magnetic entropy change (S_m) as a function of temperature.

the whole range of relaxation process. Thus, our detailed aging effects and thermoremanent magnetization study strongly support the existence of glassy state in BFSO below T_f.

3.8. Specific heat studies

Prompted by our interesting magnetization studies, we also carried out specific heat measurements on BFSO sample to understand the nature of magnetic state and magnetic entropy. The main panel of Fig. 10 depicts the temperature dependence of total specific heat (C_p) of BFSO in zero magnetic field. It is evident from the C_p vs T plot that it does not show any indication of a magnetic phase transition into long-range order (typically λ like anomaly) down to 2 K. This suggest that long-range magnetic order is absent in the BFSO. To gain further insights into the nature of phase transition, we have estimated the magnetic contribution to specific heat C_m. To estimate C_m, we have subtracted the phonon contribution from the total specific heat value. For this, we assume that in the temperature range 150-255 K range, the specific heat contribution is due to phonons only. We determine the Debye temperature (Θ_D) by least-square fitting the observed total specific heat data in the range 150–255 K using Debye equation [79]:

$$C_{lattice} = 9Nk_B\left(\frac{T}{\Theta_D}\right)^3\int_0^{\Theta_D/T}\frac{x^4e^x}{(e^x-1)^2}dx \quad (9)$$

where N_A is the Avogadro number, k_B is the Boltzmann constant, Θ_D the Debye temperature. The best fit value of Θ_D for BFSO comes out to be ≈(501 ± 5) K. After determining Θ_D, we have calculated the theoretical lattice contribution to specific heat by Eq. (9) in the temperature range 1.8–255 K. The magnetic contribution to the specific heat of BFSO was estimated by subtracting the lattice contribution from the total specific heat (see Fig. 10). It can be seen from the figure that the magnetic contribution to specific heat start growing ~150 K and around this temperature the Curie-Weiss fit and M-H curve show significant departure from the linear behaviour suggesting that some short-range correlations start developing. In dilute metallic spin-glass systems, like CuMn, AuFe, the magnetic contribution to specific heat shows linear dependence below T_f and a broad maximum above the freezing temperature T_f (at nearly 2–3 times the freezing temperature) [50]. Such a linear dependence of C_m has been explained theoretically using two level tunnelling model [80]. However, in concentrated systems, there is no unanimity about the temperature dependence of the magnetic contribution to the specific heat below T_f. Different empirical and theoretical models involving linear [81–83], exponential [84–88] and power law [89] type dependence of magnetic contribution to the specific heat have been proposed in the literature for the concentrated systems. In general, we do not expect the linear term for insulating samples at low temperatures. We believe that in our case, the linear temperature dependence of C_m below T_f (see top inset of Fig. 10) arises due to the glassy nature of the ground state. Further, it shows a broad peak ~53 K (3 times T_f) which is consistent with the well-known canonical spin-glasses [49,50].

The magnetic entropy (S_m) was estimated by integrating the C_m/T as a function of temperature using the expression [79]:

$$S_m = \int_0^T\left(\frac{C_m}{T}\right)dT \quad (10)$$

The maximum value of theoretical entropy of the system having total spin (S) can be estimated by Rln(2 S+1). So, the maximum expected theoretical entropy for Fe^{3+} ions, S = 5/2, is 14.89 J/mol-K. For BFSO, the maximum entropy value is 13.185 J/mol-K, which approximately 88% of the total theoretical magnetic entropy value. A slightly higher value of entropy may be attributed to the presence of some Fe^{4+} ions in the BFSO system. The value of entropy at T_f is found to be only 0.9 J/mol-K (see bottom inset of Fig. 10) which is approximately 3% of the total magnetic entropy. This is in broad agreement with the reported literature at which 5–15% entropy is released at T_f [50]. Thus, the temperature evolution of magnetic entropy of BFSO suggest that substantial entropy is contained in the short-range AFM correlations which are developed above the glass transition temperature. Hence, our specific heat analysis also confirms the glassy ground state of BFSO consistent with the dc and ac susceptibility studies.

3.9. Magnetic ground state of BFSO

The foregoing results indicate that BFSO exhibits cluster-glass freezing behaviour with T_G ~15.7 K and characteristic relaxation time of τ_0 ~10^{-7} s. It is well established that the percolation threshold concentration (c_p) plays a vital role in deciding the long-range order transition and short-range correlations with spin/cluster glass behaviour [90–92]. If the disorder content (c) is less than the c_p, then LRO phase transition has been observed. However, for $c > c_p$ leads to the formation of local short-range ordered FM/AFM correlated clusters with glassy behaviour [90–92]. Further, for disorder content $c \approx c_p$, a coexistence of LRO and spin/cluster-glass phases has been observed [90–92]. Since 50% of the magnetic sublattice are occupied by non-magnetic Sn^{4+} randomly in the BFSO, the absence of LRO AFM phase may be due to the randomness in exchange interaction caused by disorder. We believe that in BFSO, the disorder content ($c > c_p$) might be strong enough to stabilize the cluster glass state. However, it is worth mentioning that the percolation threshold concentration c_p varies across systems [93–96]. As explained in the earlier Section 3.2, the oxygen vacancies in the BFSO sample lead to the formation of the mixed valence states Fe^{3+} and Fe^{4+}. Recent Mössbauer spectroscopy measurements [36] also revealed the existence of mixed valence Fe^{3+} and Fe^{4+} states in BFSO. The presence of mixed valence states of Fe ions in BFSO lead to different magnetic exchange interaction pathways (Fe^{3+}- Fe^{4+}, Fe^{3+}- Fe^{3+} or Fe^{4+}- Fe^{4+}) mediated by nonmagnetic oxygen. The superexchange interaction pathways Fe^{3+}-O^{2-}-Fe^{3+} or Fe^{4+}-O^{2-}-Fe^{4+} will always be antiferromagnetic in nature while the double exchange interaction pathways Fe^{3+} -O^{2-}- Fe^{4+} will be predominantly ferromagnetic [97].

The competing nature of these two interactions induce magnetic frustration and suppresses the long-range ordering which consequently gives rise to the experimentally observed cluster glass state in BFSO. It has been shown previously [98] that the B-site disordered perovskite $Sr(Fe_{0.5}Ru_{0.5})O_3$ exhibits glassy behavior induced by the competition between Fe^{3+}-O^{2-}-Fe^{4+} ferromagnetic interaction and Fe^{3+}-O^{2-}-Fe^{3+} antiferromagnetic interaction.

It is interesting to compare our results of BFSO with the niobate perovskites $Ba(Fe_{1/2}Nb_{1/2})O_3$ (BFNO) in terms of the crystal structure, magnetic transitions and possible superexchange interaction pathways. BFNO is isostructural to BFSO i.e., it has cubic crystal structure in the $Pm\bar{3}m$ space group. The magnetic ground state of BFNO corresponds to cluster glass phase with T_G ~29 K and τ_0 ~10^{-7} s [31]. In the case of BFNO, only one superexchange interaction pathway Fe^{3+}-O^{2-}-Fe^{3+} is possible due to stable valence state of Fe^{3+}. To understand the differences in the magnetic transition temperatures of BFSO and BFNO, we compared the strength of magnetic interactions. As per Goodenough's theory of magnetic superexchange interaction [88], the magnetic interaction between $Fe^{3+}(3d^5)$ and $Fe^{3+}(3d^5)$ cations is much stronger than that between $Fe^{4+}(3d^4)$ and $Fe^{3+}(3d^5)$ cations, as well as that between $Fe^{4+}(3d^4)$ and $Fe^{4+}(3d^4)$ cations. In BFSO, the AFM superexchange interactions among the Fe^{3+}-O^{2-}-Fe^{3+} and Fe^{4}-O^{2-}-Fe^{4+} is weakened by the FM double exchange interaction through Fe^{3+}-O^{2-}-Fe^{4+} and thus leads to decrease in the transition temperature in comparison to BFNO.

Before we close, a brief comment about the possible magnetic and dielectric correlations would be in order. It is noteworthy that significant changes in the magnetic dielectric properties were observed in the vicinity of 175–200 K, for example, dielectric permittivity gradually start increasing, inverse of ZFC susceptibility deviates from the Curie-Weiss behaviour, and M-H curves changes slope, magnetic contribution to specific heat C_m start gradually increasing and the magnetic entropy change gradually decreases with lowering temperature. Thus the possibility of giant dielectric permittivity governed by the magnetic correlations cannot be ruled out in BFSO. However, more work is required using neutron diffraction and Raman scattering study and local probes like NMR to understand the role of the magnetic correlations in BFSO.

4. Conclusions

To summarize, we have synthesized polycrystalline samples of $Ba(Fe_{1/2}Sn_{1/2})O_{3-\delta}$ (BFSO) using the standard solid-state method and examined its magnetic ground state. X-ray diffraction analysis confirms that BFSO crystallizes in the cubic $Pm\bar{3}m$ symmetry. It exhibits giant dielectric permittivity ε'~10^4 at room temperature with two low temperature dielectric relaxations originating from the polaron hopping mechanism and Maxwell-Wagner effect, respectively. Temperature dependent zero-field cooled (ZFC) dc susceptibility exhibits a sharp peak at T_f ~16 K and follows Curie-Weiss behaviour well above T_f with dominant antiferromagnetic correlations (θ_{CW} ~ -(174 ± 1) K). In addition, the ZFC and field cooled (FC) χ (T) curves diverges at the irreversibility temperature T_{irr}, suggesting the glassy behaviour. Further, ac susceptibility measurements reveal frequency dispersion around T_f and a power law type critical dynamics with T_G ~15.7 K, and τ_0 ~10^{-7} s confirming the cluster glass state in BFSO. Moreover, T_f decreases with increasing field and falls on the de Almeida-Thouless line with mean field exponent m = (0.63 ± 0.09). Below T_f, we observed aging effect and magnetic relaxation behaviour due to the presence of large number of metastable states. Further, our temperature dependent specific heat measurements do not show any sharp feature in the range 2–250 K revealing the absence of long-range AFM ordering in BFSO, consistent with dc and ac magnetization studies. Interestingly, the magnetic contribution to specific heat C_m follows linear-T dependence below T_f, as expected in spin/cluster glasses. We hope that the present study would provide the key ingredients for future theoretical studies directed towards understanding the $CaCu_3Ti_4O_{12}$ type giant dielectric constant behaviour of BFSO.

5. CRediT authorship contribution statement

Arun Kumar: Conceptualization, Methodology, Formal analysis, Validation, Visualization, Writing – original draft, Writing review & editing; **Girish Sahu:** Methodology, Formal analysis, Validation; **Sunil Nair:** Supervision, Validation, Writing – review & editing.

Declaration of Competing Interest

The authors declare that they have no known competing financial interests or personal relationships that could have appeared to influence the work reported in this paper.

Acknowledgements

Arun Kumar acknowledges SERB-DST, Government of India for providing the financial support through a National Post-Doctoral Fellowship (PDF/2020/002116). We thank Dr. Surjeet Singh, IISER Pune for providing the specific heat data. Authors are thankful to Ms. Shruti Chakravarty (IISER Pune) and Dr. Vikram Singh (IISER Pune) for their help in the iodometric titration analysis.

Appendix A. Supporting information

Supplementary data associated with this article can be found in the online version at doi:10.1016/j.jallcom.2022.165914.

References

[1] S. Vaisala, M. Karppinen, $A_2B'B''O_6$ perovskites: a review, Prog. Solid State Chem. 43 (2015) 1–36.
[2] D. Serrate, J.M. De Teresa, M.R. Ibarra, Double perovskites with ferromagnetism above room temperature, J. Phys. Condens. Matter 19 (2007) 023201.
[3] R.A. Cowley, S.N. Gvasaliya, S.G. Lushnikov, B. Roessli, G.M. Rotaru, Relaxing with relaxors: a review of relaxor ferroelectrics, Adv. Phys. 60 (2011) 229.
[4] K.I. Kobayashi, T. Kimura, H. Sawada, K. Terakura, Y. Tokura, Room-temperature magnetoresistance in an oxide material with an ordered double-perovskite structure, Nature 395 (1998) 677.
[5] D. Choudhury, P. Mandal, R. Mathieu, A. Hazarika, S. Rajan, A. Sundaresan, U.V. Waghmare, R. Knut, O. Karis, P. Nordblad, D.D. Sarma, Near-room-temperature colossal magnetodielectricity and multiglass properties in partially disordered La_2NiMnO_6, Phys. Rev. Lett. 108 (2012) 127201.
[6] Y.K. Wakabayashi, Y. Krockenberger, N. Tsujimoto, T. Boykin, S. Tsuneyuki, Y. Taniyasu, H. Yamamoto, Ferromagnetism above 1000 K in a highly cation-ordered double-perovskite insulator Sr_3OsO_6, Nature, Communications 10 (2019) 535.
[7] M. Das, P. Dutta, S. Giri, S. Majumdar, Octahedral tilting and emergence of ferrimagnetism in cobalt-ruthenium based double perovskites, J. Phys. Condens. Matter 31 (2019) 385801.
[8] G.A. Smolenskii, A.I. Agranovskaia, S.N. Popov, V.A. Isupov, New ferroelectrics of complex composition $Pb_2Fe^{3+}Nb^{5+}O_6$ and Pb_2YbNbO_6, Sov, Phys. Tech. Phys. 3 (1958) 1981.
[9] G.A. Smolenskii, A.I. Agranovskaya, Dielectric polarization of a number of complex compounds, Sov. Phys. Solid State 1 (1960) 1429–1437.
[10] Y. Yang, J.M. Liu, H.B. Huang, W.Q. Zou, P. Bao, Z.G. Liu, Magnetoelectric coupling in ferroelectromagnet $Pb(Fe_{1/2}Nb_{1/2})O_3$ single crystals, Phys. Rev. B 70 (2004) 132101.
[11] R. Blinc, M. Kosec, J. Holc, Z. Trontelj, Z. Jaglicic, N. Dalal, Magnetoelectric effect in $Pb(Fe_{1/2}Nb_{1/2})O_3$, Ferroelectrics 349 (2007) 16.
[12] S.P. Singh, S.M. Yusuf, S. Yoon, S. Baik, N. Shin, D. Pandey, Ferroic transitions in the multiferroic (1-x)$Pb(Fe_{1/2}Nb_{1/2})O_3$-x$PbTiO_3$ system and its phase diagram, Acta Mater. 58 (2010) 5381.
[13] R.E. Cohen, Origin of ferroelectricity in perovskite oxides, Nature 358 (1992) 136.
[14] W. Kleemann, V.V. Shvartsman, P. Borisov, A. Kania, Coexistence of antiferromagnetic and spin cluster glass order in the magnetoelectric relaxor multiferroic $PbFe_{0.5}Nb_{0.5}O_3$, Phys. Rev. Lett. 105 (2010) 257202.
[15] S. Chillal, M. Thede, F.J. Litterst, S.N. Gvasaliya, T.A. Shaplygina, S.G. Lushnikov, A. Zheludev, Microscopic coexistence of antiferromagnetic and spin-glass states, Phys. Rev. B 87 (2013) 220403(R).
[16] V.V. Laguta, M.D. Glinchuk, M. Maryško, R.O. Kuzian, S.A. Prosandeev, S.I. Raevskaya, V.G. Smotrakov, V.V. Eremkin, I.P. Raevski, Effect of Ba and Ti

doping on magnetic properties of multiferroic $Pb(Fe_{1/2}Nb_{1/2})O_3$, Phys. Rev. B 87 (2013) 064403.
[17] S.P. Singh, D. Pandey, S. Yoon, S. Baik, N. Shin, Evidence for monoclinic crystal structure and negative thermal expansion below magnetic transition temperature in $Pb(Fe_{1/2}Nb_{1/2})O_3$, Appl. Phys. Lett. 90 (2007) 242915.
[18] I.P. Raevski, S.A. Prosandeev, A.S. Bogatin, M.A. Malitskaya, L. Jastrabik, High dielectric permittivity in $AFe_{1/2}B_{1/2}O_3$ nonferroelectric perovskite ceramics (A=Ba, Sr, Ca; B=Nb, Ta, Sb), J. Appl. Phys. 93 (2003) 4130.
[19] Z. Wang, X.M. Chen, L. Ni, X.Q. Liu, Dielectric abnormities of complex perovskite $Ba(Fe_{1/2}Nb_{1/2})O_3$ ceramics over broad temperature and frequency range, Appl. Phys. Lett. 90 (2007) 022904.
[20] Y.Y. Liu, X.M. Chen, X.Q. Liu, L. Li, Giant dielectric response and relaxor behaviors induced by charge and defect ordering in $Sr(Fe_{1/2}Nb_{1/2})O_3$ ceramics, Appl. Phys. Lett. 90 (2007) 192905.
[21] Y.Y. Liu, X.M. Chen, X.Q. Liu, L. Li, Dielectric relaxations in $Ca(Fe_{1/2}Nb_{1/2})O_3$ complex perovskite ceramics, Appl. Phys. Lett. 90 (2007) 262904.
[22] M.A. Subramanian, D. Li, N. Duan, B.A. Reisner, A.W. Sleight, High dielectric constant in $ACu_3Ti_4O_{12}$ and $ACu_3Ti_3FeO_{12}$ phases, J. Solid State Chem. 151 (2000) 323.
[23] C.C. Homes, T. Vogt, S.M. Shapiro, S. Wakimoto, A.P. Ramirez, Optical response of high-dielectric-constant perovskite-related oxide, Science 293 (2001) 673.
[24] A. Singh, A. Kumar, D. Pandey, Effect of synthesis route on structure and dielectric properties of (1-x)$BiFeO_3$-x$BaTiO_3$ solid solutions and its phase diagram, J. Appl. Phys. 124 (2018).
[25] P.D. Battle, T.C. Gibb, A.J. Herod, S.H. Kirn, P.H. Munns, Investigation of magnetic frustration in A_2FeMO_6 (A = Ca, Sr, Ba; M = Nb, Ta, Sb) by magnetometry and mössbauer spectroscopy, J. Mater. Chem. 5 (1995) 865–870.
[26] K. Tezuka, K. Henmi, Y. Hinatsu, N.M. Masaki, Magnetic susceptibilities and Mossbauer spectra of perovskites A_2FeNbO_6 (A = Sr, Ba), J. Solid State Chem. 154 (2000) 591.
[27] M. Maryško, V.V. Laguta, I.P. Raevski, R.O. Kuzian, N.M. Olekhnovich, A.V. Pushkarev, Y.V. Radyush, S.I. Raevskaya, V.V. Titov, S.P. Kubrin, Magnetic susceptibility of multiferroics and chemical ordering, AIP Adv. 7 (2017) 056409.
[28] T. Kmjec, M. Adamec, D. Kubaniova, J. Plocek, M. Dopita, M. Cesnek, V. Chlan, J. Bednarcik, K. Zaveta, M. Marysko, J. Kohout, , 57Fe-enriched perovskites M $(Fe_{0.5}Nb_{0.5})O_3$ (M – Pb, Ba) studied by Mössbauer spectroscopy, NMR and XRD in the wide temperature range 4.2–533 K, J. Magn. Magn. Mater. 475 (2019) 334–344.
[29] A. Kumar, A. Senyshyn, D. Pandey, Evidence for cluster spin glass phase with precursor short-range antiferromagnetic correlations in the B -site disordered Ca $(Fe_{1/2}Nb_{1/2})O_3$ perovskite, Phys. Rev. B 99 (2019) 214425.
[30] A. Kumar, A. Chaudhary, K. Gautam, D. Pandey, On the magnetic ground state of lead-free complex perovskite $Sr(Fe_{1/2}Nb_{1/2})O_3$, J. Alloy. Compd. 859 (2021) 157779.
[31] A. Kumar, A. Chaudhary, K. Gautam, D. Pandey, Magnetic ground state and crystal structure of the giant dielectric constant material $Ba(Fe_{1/2}Nb_{1/2})O_3$, J. Magn. Magn. Mater. 537 (2021) 168236.
[32] I.P. Raevski, S.P. Kubrin, S.I. Raevskaya, V.V. Titov, D.A. Sarychev, M.A. Malitskaya, I.N. Zakharchenko, S.A. Prosandeev, Experimental evidence of the crucial role of nonmagnetic Pb cations in the enhancement of the Néel temperature in perovskite $Pb_{1-x}Ba_xFe_{1/2}Nb_{1/2}O_3$, Phys. Rev. B 80 (2009) 024108.
[33] C.C. Homes, T. Vogt, Colossal permittivity materials: doping for superior dielectrics, Nat. Mater. 12 (2013) 782.
[34] S. Kawrani, M. Boulos, D. Cornu, M. Bechelany, From synthesis to applications: copper calcium titanate (CCTO) and its magnetic and photocatalytic properties, Chem. Open 8 (2019) 922–950.
[35] M.Y. Tse, X. Wei, J. Hao, High-performance colossal permittivity materials of (Nb + Er) co-doped TiO_2 for large capacitors and high-energy-density storage devices, Phys. Chem. Chem. Phys. 18 (2016) 24270.
[36] E.A. Bikyashev, S.P. Kubrin, A.V. Popov, A.V. Pavlenko, I.P. Raevski, N.V. Ter-Oganessian, Local environment of iron and tin ions, diffuse absorption, and giant dielectric response in $BaFe_{1/2}Sn_{1/2}O_{3-\delta}$ prepared by the sol-gel method, J. Alloy. Compd. 860 (2020) 158327.
[37] E. Lucchini, S. Meriani, D. Minichelli, An X-ray study of two phases of $BaFeO_{3-x}$, Acta Cryst. B29 (1973) 1217.
[38] A.J. Jacoson, A powder neutron diffraction study of the structure of and oxygen vacancy distribution in 6H $BaFeO_{2.79}$, Acta Cryst. B32 (1976) 1087.
[39] N. Hayashi, T. Yamamoto, H. Kageyama, M. Nishi, Y. Watanabe, T. Kawakami, Y. Matsushita, A. Fujimori, M. Takano, $BaFeO_3$: a ferromagnetic iron oxide, Angew. Chem. - Int. Ed. 50 (2011) 12547.
[40] K. Mori, T. Kamiyama, H. Kobayashi, T. Otomo, K. Nishiyama, M. Sugiyama, K. Itoh, T. Fukunaga, S. Ikeda, Mixed magnetic phase in 6H-type $BaFeO_{3-\delta}$, J. Appl. Cryst. 40 (2007) 501.
[41] A. Sagdeo, K. Gautam, P.R. Sagdeo, M.N. Singh, S.M. Gupta, A.K. Nigam, R. Rawat, A.K. Sinha, H. Ghosh, T. Ganguli, A. Chakrabarti, Large dielectric permittivity and possible correlation between magnetic and dielectric properties in bulk $BaFeO_{3-\delta}$, Appl.Phys.Lett. 105 (2014) 042906.
[42] R. Ahmed, S.T. Wang, J. Sun, J. Wang, T.Y. Li, Y. Yu, Q.J. Li, C.C. Wang, Colossal dielectric behavior in $BaFeO_{3-\delta}$ ceramics, Ceram. Int. 45 (2019) 13484.
[43] N.T. Dang, D.P. Kozlenko, N. Tran, B.W. Lee, T.L. Phan, R.P. Madhogaria, V. Kalappattil, D.S. Yang, S.E. Kichanov, E.V. Lukin, B.N. Savenko, P. Czarnecki, T.A. Tran, V.L. Vo, L.T.P. Thao, D.T. Khan, N.Q. Tuan, S.H. Jabarov, M.H. Phan, Structural, magnetic and electronic properties of Ti-doped $BaFeO_{3-\delta}$ exhibiting colossal dielectric permittivity, J. Alloy. Compd. 808 (2019) 151760.
[44] F. Iga, Y. Nishihara, G. Kido, Y. Takeda, M6ssbauer effect and high-field magnetization of $BaFeO_{3-y}$, J. Magn. Magn. Mater. 104 (1992) 1969.
[45] K.S. Roh, M.G. Kim, K.S. Ryu, C.H. Yo, Nonmetallic spin glass behavior by spin frustration at low temperature in nonstoichiometric $BaSn_{1-x}Fe_xO_{3-y}$ system, Solid State Commun. 100 (1996) 565.
[46] E.A. Bikyashev, A.V. Popov, S.P. Kubrin, P. Yanda, M.B. Mayorov, A. Trigub, V.A. Shuvaeva, A. Sundaresan, I.P. Raevski, N.V. Ter-Oganessian, Magnetic and dielectric properties of $BaFe_{1/2}Sn_{1/2}O_{3-\delta}$ ceramics, Ceram. Int. 48 (2022) 7951.
[47] S. Bedanta, W. Kleemann, Supermagnetism, J. Phys. D: Appl. Phys. 42 (2009) 013001.
[48] C. Sow, D. Samal, P.S.A. Kumar, A.K. Bera, S.M. Yusuf, Structural-modulation-driven low-temperature glassy behavior in $SrRuO_3$, Phys. Rev. B 85 (2012) 224426.
[49] K. Binder, A.P. Young, Spin glasses: expeimental facts, theoretical concepts, and open questions, Rev. Mod. Phys. 58 (1986) 801–976.
[50] J.A. Mydosh, Spin glasses: redux: an updated experimental/materials survey, Rep. Prog. Phys. 78 (2015) 052501.
[51] H. Kawamura, T. Taniguchi, "Spin Glasses", in: K.H.J. Bischow (Ed.), Hand Book of Magnetic Materials, Elsevier, Amsterdam, 2015.
[52] J.R. Carvajal, Laboratary, FULLPROF, A Rietveld amd pattern matching and analysis program, Laboratary Leon Brillouin, CEA-CNRS, France, 2010.
[53] G.K. Williamson, W.H. Hall, X-ray line broadening from filed Al and W, Acta Metall. 1 (1953) 22–31.
[54] A. Kumar, P. Singh, R.J. Chdudhary, D. Pandey, Effect of Mn-doping on the low temperature magnetic phase transition of $BiFeO_3$, J. Alloy. Compd. 825 (2020) 154148.
[55] B.D. Culity, Introduction to Magnetic Materials, Addison-Wesely, Publishing Compnay Inc., Philippin, 1972.
[56] M.D. Mukadam, S.M. Yusuf, P. Sharma, S.K. Kulshreshtha, G.K. Dey, Dynamics of spin clusters in amorphous Fe_2O_3, Phys. Rev. B 72 (2005) 174408.
[57] P. Bag, P.R. Baral, R. Nath, Cluster spin-glass behavior and memory effect in $Cr_{0.5}Fe_{0.5}Ga$, Phys. Rev. B 98 (2018) 144436.
[58] T. Chakrabarty, A.V. Mahajan, S. Kundu, Cluster spin glass behavior in geometrically frustrated $Zn_3V_3O_8$, J. Phys.: Condens. Matter 26 (2014) 405601.
[59] M.A.V. Heringer, D.L. Mariano, D.C. Freitas, E. Baggio-Saitovitch, M.A. Continentino, D.R. Sanchez, Spin-glass behavior in $Co_3Mn_3(O_2BO_3)_2$ ludwigite with weak disorder, Physical Review, Materials 3 (2020) 064412.
[60] T. Naka, T. Nakane, S. Ishii, M. Nakayama, A. Ohmura, F. Ishikawa, A. De Visser, H. Abe, T. Uchikoshi, Cluster glass transition and relaxation in the random spinel $CoGa_2O_4$, Phys. Rev. B 103 (2021) 224408.
[61] B. Venkateswarlu, R. Hari Krishnan, J. Arout Chelvane, P.D. Babu, N. Harish, Kumar, Coexistence of cluster ferromagnetism and cluster spin-glass like behaviour in melt-quenched $Cu_2Mn_{0.5}Fe_{0.5}Al$ Heusler alloy, J. Alloy. Compd. 777 (2019) 373.
[62] M.H. Phan, N.A. Frey, H. Srikanth, M. Angst, B.C. Sales, D. Mandrus, Magnetism and cluster glass dynamics in geometrically frustrated $LuFe_2O_4$, J. Appl. Phys. 105 (2009) 07E308.
[63] S. Kundu, T. Dey, A.V. Mahajan, N. Büttgen, $LiZn_2V_3O_8$: a new geometrically frustrated cluster spin-glass, J. Phys.: Condens. Matter 32 (2020) 115601.
[64] M.K. Warshi, A. Kumar, A. Sati, S. Thota, K. Mukherjee, A. Sagdeo, P.R. Sagdeo, Cluster glass behavior in orthorhombic $SmFeO_3$ perovskite: interplay between spin ordering and lattice dynamics, Chem. Mater. 32 (2020) 1250.
[65] R. Pradheesh, H.S. Nair, C.M.N. Kumar, J. Lamsal, R. Nirmala, P.N. Santhosh, W.B. Yelon, S.K. Malik, V. Sankaranarayanan, K. Sethupathi, Observation of spin glass state in weakly ferromagnetic Sr_2FeCoO_6 double perovskite, J. Appl. Phys. 111 (2012) 053905.
[66] M. Hadouchi, A. Assani, M. Saadi, Y. Kopelevich, R.R. da Silva, A. Lahmar, H. Bouyanfif, M. El Marssi, L. El, Ammari, Unconventional spin-glass-like state in $AgCo_2V_3O_{10}$, the novel magnetically frustrated material, J. Magn. Magn. Mater. 491 (2019) 165623.
[67] E. Vincent, V. Dupuis, Spin glasses: Experimental signatures and salient outcomes, Springe Ser. Mater. Sci. 275 (2018) 31–56.
[68] J.R.L. de Almeida, D.J. Thouless, Stability of the Sherrington-Kirkpatrick solution of a spin glass model, J. Phys. A: Math. Gen. 11 (1978) 983.
[69] D.S. Fisher, D.A. Huse, Nonequilibrium dynamics of spin glasses, Phys. Rev. B 38 (1988) 373–385.
[70] D.M. Cragg, D. Sherrington, M. Gabay, Instabilities of an m-Vector Spin-Glass in a Field, Phys. Rev. Lett. 49 (1982) 158.
[71] M. Gabay, G. Toulouse, Coexistence of spin-glass and ferromagnetic orderings, Phys. Rev. Lett. 47 (1981) 201.
[72] W. Sun, P. Cheng, Y. Fang, B. Kang, W. Lu, S. Cao, J. Zhang, F. Chen, Re-entrant spin-glass behavior induced by co-doping in hexagonal $Y_{0.3}Lu_{0.7}MnO_3$ single crystal, J. Alloy. Compd. 838 (2020) 155582.
[73] A. Kumar, S.D. Kaushik, V. Siruguri, D. Pandey, Evidence for two spin-glass transitions with magnetoelastic and magnetoelectric couplings in the multiferroic $(Bi_{1-x}Ba_x)(Fe_{1-x}Ti_x)O_3$ system, Phys. Rev. B 97 (2018) 104402.
[74] A.K. Khorwal, S. Dash, Nancy, A. Kumar, A.V. Lukoyanov, E.I. Shreder, Y. Bitla, M. Vasundhara, A.K. Patra, Evidence for canonical spin glass behaviour in polycrystalline Mn 1. 5 Fe 1. 5 Al Heusler alloy, J. Magn. Magn. Mater. 546 (2021) 168752.
[75] R.G. Palmer, D.L. Stein, E. Abrahams, P.W. Anderson, Models of hierarchically constrained dynamics for glassy relaxation, Phys. Rev. Lett. 53 (1984) 958–961.
[76] P.A. Kumar, A. Kumar, K. Kumar, G.A. Babu, P. Vijayakumar, S. Ganesamoorthy, P. Ramasamy, D. Pandey, Evidence for spin glass transition in hexagonal $DyMnO_3$ without substitutional disorder, J. Phys. Chem. C. 123 (2019) 30499.
[77] Y. Yeshurum, L.J.P. Ketelsen, M.B. Salamon, Experimental study of the temperature-field phase diagram of spin-glasses, Phys. Rev. B 26 (1982) 1491–1494.

[78] A. Kumar, D. Pandey, Study of magnetic relaxation, memory and rejuvenation effects in the cluster spin-glass phase of B -site disordered $Ca(Fe_{1/2}Nb_{1/2})O_3$ perovskite: Experimental evidence for hierarchical model, J. Magn. Magn. Mater. 511 (2020) 166964.
[79] E.S.R. Gopal, Specific Heat at Low Temperatures, Plenun Press, New York, 1966.
[80] P.W. Anderson, B.I. Halperin, C.M. Varma, Anomalous low-temperature thermal properties of glasses and spin glasses, Philos. Mag. 25 (1971) 1.
[81] D. Meschade, F. Steglich, W. Felsch, H. Maletta, W. Zinn, Specific heat of insulating spin-glasses, (Eu,Sr)S, near the onset of ferromagnetism, Phys. Rev. Lett. 44 (1980) 102.
[82] H. v Lohnesysen, R. van den Berg, G.V. Lecomte, W. Zinn, Specific heat of $Eu_xSr_{1-x}S$ in high magnetic fields, Phys. Rev. B. 31 (1985) 2920.
[83] K. Westerholt, H. Endrikat, R. Dahlbeck, H. Bach, J.M. Friedt, Magn. phase Diagr. EuxLa1−xS Phys. Rev. B 33 (1986) 567.
[84] A.D. Maestro, M.J.P. Gingras, Low-temperature specific heat and possible gap to magnetic excitations in the Heisenberg pyrochlore antiferromagnet $Gd_2Sn_2O_7$, Phys. Rev. B 76 (2007) 064418.
[85] J.A. Quilliam, K.A. Ross, A.G. Del Maestro, M.J.P. Gingras, L.R. Corruccini, J.B. Kycia, Evidence for gapped spin-wave excitations in the frustrated $Gd_2Sn_2O_7$ pyrochlore antiferromagnet from low-temperature specific heat measurements, Phys. Rev. Lett. 99 (2007) 097201.
[86] J.C. Lashley, R. Stevens, M.K. Crawford, J. Boerio-Goates, B.F. Woodfield, Y. Qiu, J.W. Lynn, P.A. Goddard, R.A. Fisher, Specific heat and magnetic susceptibility of the spinels $GeNi_2O_4$ and $GeCo_2O_4$, Phys. Rev. B. 78 (2008) 104406.
[87] J.A. Morrison, D.M.T. Newsham, Analyses of low-temperature heat capacities containing two or more contributions: application to the rare earth metals, J. Phys. C. Solid State Phys. 1 (1968) 370.
[88] A. Schroder, H. v Lohneysen, W. Bauhofer, Magnetic susceptibility and specific heat of an anisotropic spin-glass: $Eu_xSr_{1-x}As_3$, Phys. Rev. Lett. 57 (1986) 622.
[89] R. Caudron, P. Costa, B. Levesque, Power law behaviour for the specific heat of spin glasses at very low temperatures, J. Phys. F. Met. Phys. 11 (1981) 451.
[90] A.B. Harris, Effect of random defects on the critical behaviour of Ising models, J. Phys. C: Solid State Phys. 7 (1974) 1671.
[91] V.K.S. Shante, S. Kirkpatrick, An introduction to percolation theory, Adv. Phys. 20 (1971) 325–357.
[92] M.F. Sykes, J.W. Essam, Critical percolation probabilities by series methods, Phys. Rev. 133 (1964) A310.
[93] H. Yoshizawa, S. Mitsuda, H. Aruga, A. Ito, Mixed phase of spin-glass ordering and antiferromagnetism in an Ising system, $Fe_xMn_{1-x}TiO_3$, Phys. Rev. Lett. 59 (1987) 2364–2367.
[94] P.Z. Wong, S. Von Molnar, T.T.M. Palstra, J.A. Mydosh, H. Yoshizawa, S.M. Shapiro, A. Ito, Coexistence of Spin-Glass and Antiferromagnetic Orders in the Ising System $Fe_{0.55}Mg_{0.45}Cl_2$, Phys. Rev. Lett. 55 (1985) 2043–2046.
[95] J. Lauer, W. Keune, Magnetic Double Transition in Au-Fe Near the Percolation Threshold, Phys. Rev. Lett. 48 (1982) 1850–1853.
[96] D.H. Ryan, Recent Progress in Random Magnets, World Scientific, Singapore, 1992.
[97] J.B. Goodenough, Magnetism and chemical bond, Wiley, New York, London, 1963.
[98] P. Battle, T.C. Gibb, C.W. Jones, F. Studer, Spin glass behaviour in Sr_2FeRuO_6 and $BaLaNiRuO_6$: a comparison with antiferromagnetic $BaLaZnRuO_6$, J. Solid. State Chem. 78 (1989) 281.